# Phase change surfaces with porous metallic structures for long-term anti/de-icing application

*Deyu Yang* [a], *Rui Bao* [b], *Adam T. Clare* [c], *Kwing-So Choi* [c], *Xianghui Hou* [a,*]

[a] State Key Laboratory of Solidification Processing, Shaanxi Key Laboratory of Fiber Reinforced Light Composite Materials, Northwestern Polytechnical University, Xi'an 710072, China.

[b] Faculty of Materials Science and Engineering, Kunming University of Science and Technology, Kunming, 650500, China.

[c] Faculty of Engineering, University of Nottingham, Nottingham, NG7 2RD, UK

*Corresponding Author: Prof. Xianghui Hou, E-mail: houxianghui@nwpu.edu.cn.

## Abstract

*Hypothesis:* Ice mitigation has received increasing attention due to the severe safety and economic threats of icing hazards to modern industries. Slippery icephobic surface is a potential ice mitigation approach due to its ultra-low ice adhesion strength, great humidity resistance, and effective delay of ice nucleation. However, this approach currently has limited practical applications because of serious liquid depletion in the icing/de-icing process.

*Experiments:* A new strategy of phase change materials (PCM)-impregnation porous metallic structures (PIPMSs) was proposed to develop phase changeable icephobic surfaces in this study, and aimed to solve the rapid depletion via the phase changeable interfacial interactions.

*Findings:* Evaluation of surface icephobicity and interfacial analysis proved that the phase changeable surfaces (PIPMSs) worked as an effective and durable icephobic platform by significantly delaying ice nucleation, providing long-term humid tolerance, low ice adhesion strength of as-prepared samples (less than 5 kPa), and signally improved maintaining capacity of impregnated PCMs (less than 10% depletion) after 50 icing/de-icing cycles. To explore the interfacial responses, phase change models consisting of the unfrozen quasi-liquid layer and solid lubricant layer at the ice/PIPMSs interfaces were established, and the involved icephobic mechanisms of PIPMSs were studied based on the analysis of interfacial interactions.

**Keywords:** phase changeable surfaces, icephobic, interfacial interactions, solid lubricant, quasi-liquid layer.

## Abbreviations

CCO: coconut oil; CCO/Cu: Porous Cu structure with the impregnation of coconut oil; CCO/POTS: POTS coated structure with the impregnation of coconut oil; CCO/PW: Paraffin wax coated structure with the impregnation of coconut oil; DSC: differential scanning calorimetry; ESEM: environmental scanning electron microscope; LPEG: polyethylene glycol with 200 molecular weight; LPEG/Cu: Porous Cu structure with the impregnation of LPEG; LPEG/POTS: POTS coated structure with the impregnation of LPEG; LPEG/PW: Paraffin wax coated structure with the impregnation of LPEG; PCM: phase change materials; P/Cu: porous Cu structure; PEG: polyethylene glycol with 2000 molecular weight; PEG/Cu: Porous Cu structure with the impregnation of PEG; PEG/POTS: POTS coated structure with the impregnation of PEG; PEG/PW: Paraffin wax coated structure with the impregnation of PEG; PIPMSs: PCM-impregnation porous metallic structures; PMMA: poly(methyl methacrylate); PO: peanut oil; PO/Cu : Porous Cu structure with the impregnation of peanut oil; PO/POTS: POTS coated structure with the impregnation of peanut oil; PO/PW: Paraffin wax coated structure with the impregnation of peanut oil; POTS: 1H, 1H, 2H, 2H-perfluorooctyltriethoxysilane; POTS/Cu: POTS coated porous structure; PW: paraffin wax; PW/Cu: Paraffin wax coated porous structure; SEM: scanning electron microscope; SLIPS: slippery liquid-infused porous surface; WCA: water contact angle.

## 1. Introduction

Icing hazards have drawn increasing attention due to the safety and economic challenges for aviation, wind turbine generation, and other industries that face icing environments [1-6]. Hundreds of accidents or even fatalities in the aviation industry have been reported that linked to the accretion of ice on aircraft surfaces [7, 8]. To solve the above concerns, many ice protection techniques, from active methods with the consumption of external energy or chemical agents to various passive icephobic surfaces, have been developed in recent years [9-13]. Slippery liquid-infused porous surface (SLIPS) is one of the popular routes for ice mitigation due to its ultra-low ice adhesion strength, great humidity resistance, and capability of delaying ice nucleation [14-16]. The critical issue of SLIPSs is to maintain the infused liquids that keep the icing initiation position on the floating and smooth liquid surfaces instead of on the solid surfaces [17]. The attachment of surface ice blocks and the ice nucleation are restrained accordingly [18]. However, because of the harsh environmental conditions and numerous icing/de-icing operations in practice, current icephobic SLIPSs always lose the icephobic properties rapidly with the depletion of infused liquid [19, 20]. Also, most reported SLIPSs are designed using soft porous polymer structures, which are mechanically vulnerable for real applications [21, 22].

Some efforts have been made to solve the above problems of SLIPSs by the optimisation of porous structures [23-25]. Mahmut et al. reported a kind of polymer-based SLIPSs with ultra-high porosity to enhance the maintaining capacity of infused liquid to lengthen the icephobic performance [26]. Araz et al. proposed a durable multi-layer slippery icephobic structure, of which the ice adhesion strength was kept at a low value even after more than 100 days or after 50 icing/de-icing cycles [27]. Improved slippery icephobic surfaces were also reported to overcome the intrinsic deficiencies of SLIPSs [28-30]. However, current solutions still do not address the bottleneck issues for the real applications of slippery icephobic surfaces, especially in the depletion of infused lubricants. In our previous research, porous metal-based slippery icephobic structures with hydrophobic/oleophilic guarding designs were proposed to prepare durable slippery icephobic surfaces with good mechanical durability [31]. The optimisation of porous structure (including improving structural design and surface functionalisation) achieved a great extension of icephobic lifetime with the enhancement of interaction between the infused liquids and the porous surfaces. However, the liquid depletion issue was still not satisfactory. Considering the current infused liquids are mainly nonfrozen lubricants (in liquid phase at subzero temperature) or anti-freezing agents (mutually soluble with water), two research directions can be considered in SLIPSs which are reducing the mobility of lubricants and decreasing the solubility of anti-freezing agents. Phase change materials (PCMs) refer to materials that have at least two variable phases, such as amorphous and crystalline phases, while the phase change is reversible [32]. The current applications of PCM in ice mitigation mainly follow the concepts of using PCM microcapsules that achieve effective icing delay by the release of the PCM latent heat [33-37]. Shamshiri et al. reported a series of PCM encapsulated icephobic coatings, using the mixtures of n-dodecane and n-tetradecane as the phase change candidates (freezing point around 0 ℃) [38]. The PCM latent heat was utilised to obtain markedly icing delay through a modified differential scanning calorimetry (DSC) process (cooling from 40 to − 40 ℃ at a 5 K/min rate) [39]. The use of PCM latent heat is more suitable for the situation that faced the environmental temperature decreasing to subzero in a short period. Thus, for long-term usage, the PCM latent heat was not taken into consideration in the microstructural design this time.

In this study, to develop icephobic surfaces which support tailorable interfacial interactions, a strategy of phase change materials (PCM)-impregnation porous metallic structures (PIPMSs) is proposed by impregnating PCMs into porous metallic structures. Long-term icephobicity and good maintaining capacity of impregnated PCMs have been proved by anti/de-icing evaluations, while the involved icephobic mechanisms at the ice/solid interfaces have been proposed and investigated with interfacial interaction models consisting of unfrozen quasi-liquid layer and solid lubricant layer.

## 2. Method

### 2.1 Raw materials

Atomized Cu powder (average size of around 45 μm) was obtained from Inoxia Ltd. 1H, 1H, 2H, 2H-perfluorooctyltriethoxysilane (POTS), paraffin wax (PW) (mp 58-62°C), polyethylene glycol-200 (LPEG), polyethylene glycol-2000 (PEG), peanut oil (PO), and coconut oil (CCO) were purchased from Merck Life Science UK Ltd. All the chemicals were used as received.

Four typical PCMs, polyethylene glycol with 200 molecular weight (LPEG, viscous liquid), polyethylene glycol with 2000 molecular weight (PEG), peanut oil (PO), and coconut oil (CCO), were chosen as the impregnated candidates. LPEG and PEG were chosen as anti-freezing PCMs as LPEG was in the liquid phase and PEG existed in the solid phase at both room and subzero temperatures. Compared to the commonly used liquid anti-freezing agent (ethylene glycol), LPEG and PEG (with longer molecular chains) reduced the number of exposed hydrogen atoms and hydroxyls to form hydrogens bond with hydrones. Thus, the water solubility sequence was PEG < LPEG < ethylene glycol. PO and CCO were used as solid lubricants due to that both of them were in the solid phase at subzero temperature. However, PO became a yellow liquid due to the lower freezing point than CCO. The detailed physical properties of all the PCMs are given in Table S1 in the supporting information.

### 2.2 Preparation of PIPMSs

The schematic illustration of the preparation of PIPMSs is shown in Figure 1. Hydraulic press machining (a die with 20 mm inner diameter at 400 MPa for 5 minutes) and vacuum sintering processes (sintered at 800 °C and $10^{-5}$ mbar for 1 hour) were performed to fabricate the porous Cu structures. Two surface functionalization approaches were used separately to enhance the water repellency and the absorption capacity of PCM in the porous structures. Part of the as-prepared porous structures were placed into a sealed beaker with 0.3 ml POTS and underwent a CVD process to deposit a monolayer of POTS, while the PW-treated structures were obtained by immersing porous Cu structures into the PW solutions (PW:xylene=1:17, xylene was used to ensure that the layer of PW was thin enough to keep the original porosity) under 10 mbar pressure for 10 mins followed by a drying process at room temperature for 24h. The monolayer structure of POTS and low concentration of PW solution were applied to keep the original porosity and the porous structure, which was beneficial for the impregnation of PCMs and long-term icephobicity. The porous Cu structure (P/Cu), POTS-treated porous Cu structure (POTS/Cu), and PW-treated porous Cu structure (PW/Cu)) were obtained after the surface functionalisation. With the POTS- and PW-treatments, the results in this study were comparable to those from our previous work and references, which would be helpful to clarify the advances and effectiveness of the phase changeable icephobic surfaces. The microstructural information, hydrophobicity, and lipophilicity of the above three porous structures were summarised in Figure S1 in the supporting information. The detailed parameters for preparing the porous metallic structures and surface functionalisation were also described in the supporting information. The porosities, surface roughness, and mechanical properties of porous Cu structures were listed in Table S2 of the supporting information.

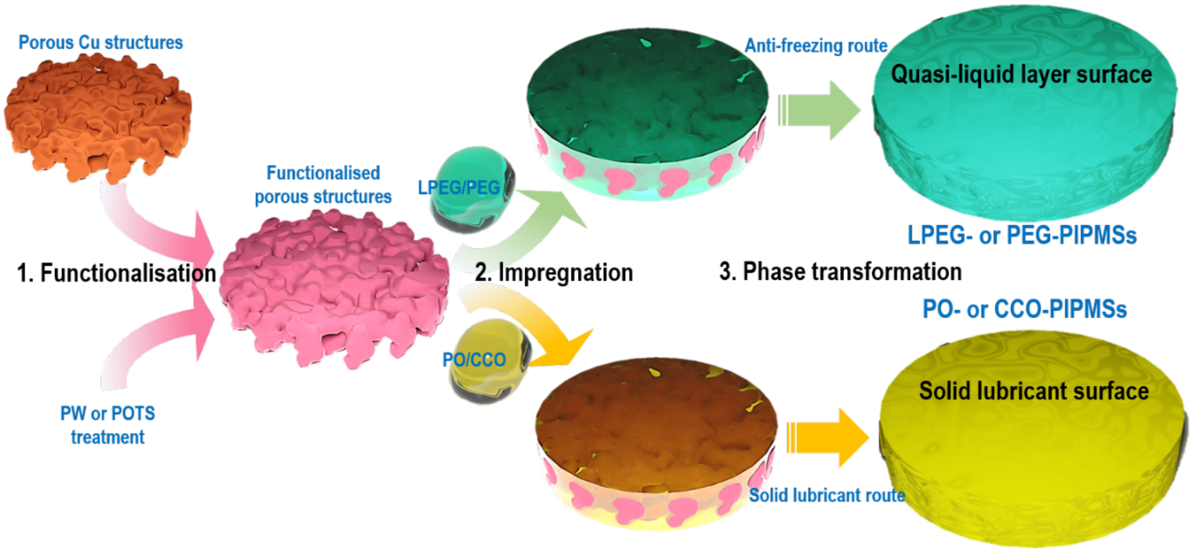

**Figure 1** Schematic illustration of the preparation of PIPMSs.

The coconut oil (CCO) and polyethylene glycol-2000 (PEG) were placed in a beaker at 55°C to obtain the liquid phase, respectively. Then porous Cu structures were immersed and the beaker was transferred into a vacuum furnace with a pressure of 10 mbar and a temperature of 55°C for 30 minutes. Similar processes were performed with peanut oil (PO) and polyethylene glycol-200 (LPEG) at room temperature. Subsequently, all the samples were removed from the beaker and placed vertically for 10 minutes to minimize the influence of liquid/solid interfacial tension and obtain a homogeneous thickness of an over-covered liquid layer. Then all the samples were placed at room temperature for 5 hours to obtain the final PIPMSs. For convenience, the description and abbreviation of the obtained samples are summarised in Table 1.

**Table 1** Description and abbreviation of porous metallic structures and PIPMSs.

| Description | Abbreviation |
|---|---|
| porous Cu structure | P/Cu |
| POTS coated porous structure | POTS/Cu |
| Paraffin wax coated porous structure | PW/Cu |
| Porous Cu structure with the impregnation of coconut oil | CCO/Cu |
| POTS coated structure with the impregnation of coconut oil | CCO/POTS |
| Paraffin wax coated structure with the impregnation of coconut oil | CCO/PW |
| Porous Cu structure with the impregnation of peanut oil | PO/Cu |
| POTS coated structure with the impregnation of peanut oil | PO/POTS |
| Paraffin wax coated structure with the impregnation of peanut oil | PO/PW |
| Porous Cu structure with the impregnation of LPEG | LPEG/Cu |
| POTS coated structure with the impregnation of LPEG | LPEG/POTS |
| Paraffin wax coated structure with the impregnation of LPEG | LPEG/PW |
| Porous Cu structure with the impregnation of PEG | PEG/Cu |
| POTS coated structure with the impregnation of PEG | PEG/POTS |
| Paraffin wax coated structure with the impregnation of PEG | PEG/PW |

### 2.3 Characterisation of surface properties

The 3D surface topography and surface roughness of the as-prepared and tested PIPMSs were characterised by a Zeta-20 non-contact profilometer. A contact angle goniometer (FTA200, First Ten Angstorms, Inc., Portsmouth, VA, USA) was used to evaluate the water contact angle (WCA) before and after the repeated icing/de-icing tests, of which water pumping out rate was set at 2 μL/s. Each sample was measured 3 times on different positions to obtain the averages as the final values of WCA. An FEI Quanta 650 ESEM was used to observe water condensation and ice formation on the sample surface in-situ. The ESEM platform was developed from a scanning electron microscope (SEM) with a water-cooled Peltier that could reach subzero temperature and a gaseous secondary electron detector (GSED) to characterise the surface condensation/icing at a relatively higher pressure. The ESEM characterisation was performed with a 15 kV voltage and a spot size of 4.5. The distance between the detector and the samples was 10 mm. To initiate the nucleation of water and ice on the surface, the temperature of the Peltier was adjusted in the range from -6 to -7 °C, and the pressure was adjusted from 360 to 500 Pa.

### 2.4 Evaluation of icephobic performance

**Aerosol icing test:** The Aerosol icing test is a simulation of the icing process in a cold chamber with constant airflow at subzero temperatures [40-42]. The cold chamber was made of a cold plate (Para Cooler A, Para Cooler O, Weinkauf Medizintechnik, Germany) with a transparent and sealed poly(methyl methacrylate) (PMMA) cover to form a thermally insulated space. The aerosol (tiny supercooled water droplets) was led to the cold chamber at a constant volumetric flow rate by an atomizer (Omron Ultrasonic Nebulizer NE-U17). To obtain better contact between samples and aerosol, the samples were placed on a rotary holder at 45° along the horizontal direction. The details of the experimental set-up can be found in Figure S2 in the supporting information. After a 20-minute pre-cooling process, the icing simulation was performed at -6.5 °C with 99% relative humidity, where the sample was rotated at an angular velocity of 0.5 rad/s. The icing process for each sample lasted for 20 minutes and was repeated 20 times. After each test, the iced samples were removed from the rotary holder to capture the image of ice accretion on the top surfaces to investigate the anti-icing performance of each sample.

**Water droplet icing test:** Water droplet icing test was also conducted in the cold chamber with a temperature of -10 °C and a relative humidity of 30% without airflow. All the samples were placed in the chamber to cool down for 20 minutes in advance. Then, a deionized water droplet (volume of 60 μl) was added to the surface to initiate the icing process. The icing processes were recorded by a digital video camera. The icing phenomena and icing time were extracted from each video. The longest recording time was 10 minutes even though the icing still did not happen.

**Ice adhesion strength:** The measurement of ice adhesion strength was performed in the same cold chamber for the aerosol icing test, with the operational temperature of -10 ℃. A semi-ellipsoidal shaped rubber mold with deionized water was used to produce a block of ice on the test surfaces. After a 10 h icing process, uniform ice blocks were formed on each sample which was ready for the ice adhesion strength test. The shear force setup and calculation of ice adhesion strength can be found in Figure S3 supporting information. To minimise experimental errors, three identical samples were tested for each kind of PIPMS and the averages were used as final values. The tests were repeated 50 times to evaluate the icephobic durability. One icing/de-icing cycle lasted for about 10 hours at -10 ℃. After each cycle, the fracture surface of the ice detachment was captured and the weights of the samples were recorded within a quite short time at -10 ℃.

## 3. Results and discussions

### 3.1 Water condensing and ice nucleation on the porous metallic structures

To explore the anti/de-icing mechanism of the phase changeable surfaces of PIPMSs, it is necessary to examine the water condensing and ice nucleating/growing behaviour of the porous metallic structures. Figure 2a showed the water condensing process on the dry porous Cu structure, where the condensation started in the gaps between Cu particles. With the effect of gravity and surface tension, the liquid water filled in the gaps and covered the lower part first. Then further condensation led to a full wetting of the entire structure. A similar process occurred when icing started in the gaps or pores of the porous surface in Figure 2b. Due to the isotropy of the porous metallic structures, further ice growth took place from the nucleation sites in all directions until the full coverage with ice. This nucleation behaviour agreed with the theory of heterogeneous nucleation that the surface morphology affected the heterogeneous nucleating free energy ($\Delta G^*$), governed by [11, 43]:

$$\Delta G^* = \frac{16\pi\gamma_{IW}^3}{3\Delta G_V^2} f(m, x) \tag{1}$$

$$m = \cos\theta = \frac{\gamma_{SW} - \gamma_{SI}}{\gamma_{WI}} \tag{2}$$

$$x \ (= \frac{R}{r_c}) \tag{3}$$

where $\gamma_{SW}$, $\gamma_{SI}$, and $\gamma_{WI}$ are the surface energy values of solid-water, solid-ice, and water-ice interface, respectively. $m$ was determined by the surface energy of the interfaces, while $x$ is related to the radius of features of the surface ($R$) and the critical nucleolus radius ($r_c$). In this study, the rough edges of Cu powders had a low heterogeneous nucleating free energy barrier with earlier nucleation and faster nucleation rates. Due to the full filling of gaps with condensed water or nucleated ice, the above phenomena indicate mechanical interlocking at the ice/structure interface on the porous metallic structures. This is strong evidence to show that dry icephobic surfaces are easy to lose their icephobic properties in high-humidity environments. The transformation of ice initiation position from solid surfaces to the PCM surfaces has the potential to lead to effective phase changeable interfacial interactions, which has a high possibility of reducing the mechanical interlocking and further delaying ice nucleation and lowering ice adhesion strength.

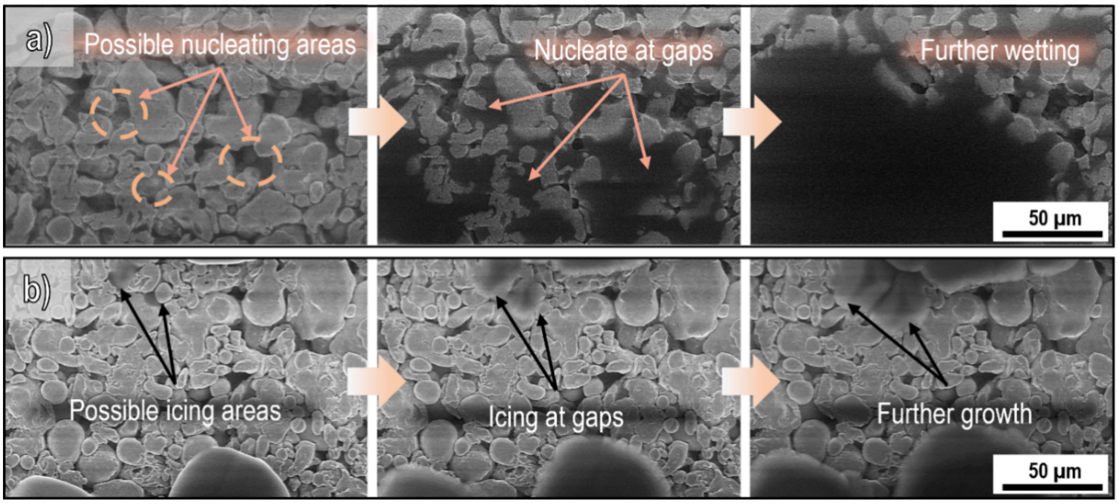

**Figure 2** ESEM characterisation of the process for (a) water condensation and (b) ice nucleation and growth on dry porous Cu structures.

### 3.2 Aerosol icing behaviours of PIPMSs

All the icing phenomena of PIPMSs in aerosol icing experiments were categorized into four types. Figure 3 illustrates these icing phenomena (icing on LPEG, PEG, SO, and CCO respectively) during the aerosol icing experiments. Firstly, for the oil-PIPMSs (both PO and SO), severe ice accretion happened on the surfaces during the 20 repeated tests, demonstrating that the oil-PIPMSs do not have good anti-icing performance.

For the LPEG and PEG samples, after icing, clear liquid trails were observed on the as-prepared surfaces due to the phase changeable interfacial interactions among ice, supercooled water, LPEG, and PEG. The dissolution of LPEG and PEG decreased the freezing point which led to the existence of the unfrozen quasi-liquid layer. However, the anti-icing performance of LPEG-PIPMSs was lost within several icing times. After the 1st icing process, for example, some tiny ice crystals were observed at the edges of the surface when the main surface was covered with evident liquid trails. After the 10th icing, no liquid trails appeared on the surface, while the ice accretion was still much weaker than that on oil-PIPMSs. After 20 icing times, however, the ice accretion became similar to that on oil surfaces, where a thick ice layer was formed without any liquid trails. The quasi-liquid layer receded under the surface of porous structures. The ice accretion on PEG-PIPMSs was much weaker than that on LPEG-PIPMSs, as shown in the second column of Figure 3. In the beginning, only small liquid trails were formed on the surface, while part of the semi-melted ice crystals occurred on the surface after the 10th icing. Even after 20 icing/de-icing cycles, liquid trails and a large amount of semi-melted ice crystals were observed on the PEG-PIPMSs surface. The amount of surface ice was also much less than other groups. To reduce the liquid depletion by infusing PCM, the phase changeable surfaces consisting of the solid anti-freezing agent (PEG) performed much better than that of the viscous liquid (LPEG). The limited dissolution of PEG and solid properties ensured the reduced consumption of PEG from both less dissolution and less depletion during the removal of ice. Thus, it is suggested that good PCM maintaining capacity with long-term and good humid icing tolerance was achieved from this investigation.

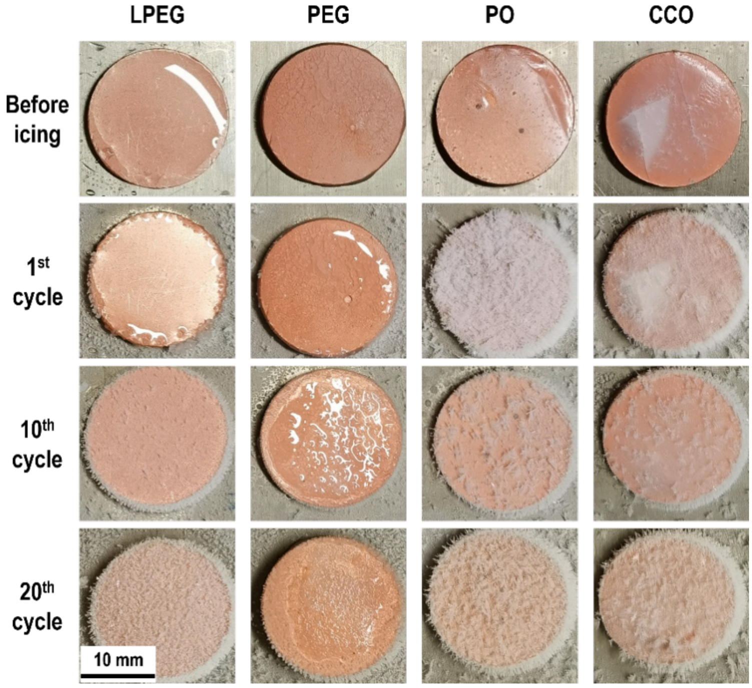

**Figure 3** Accretion of rime ice on various PIPMSs in 20 cycles of aerosol icing experiment.

### 3.3 Evaluation of ice adhesion strength

Figures 4a to 4c summarise the ice adhesion strength of Cu-based, POTS-based, and PW-based PIPMSs and the corresponding porous metallic structures during 50 icing/de-icing cycles. For the as-prepared PIPMSs, the LPEG-impregnated samples always had the lowest ice adhesion strength (around 5 kPa), while the others ranked from low to high ice adhesion strength were PEG, PO, and CCO. This result indicated that the phase changeable interfacial interactions of LPEG and PEG formed an unfrozen quasi-liquid layer and reduced the ice adhesion strength. The solid lubricating effect of PO and CCO surfaces was relatively weaker than the unfrozen liquid layer, causing higher ice adhesion. Meanwhile, due to the liquid nature and better solubility, LPEG had lower ice adhesion than PEG of the as-prepared samples. PO had a lower melting point than CCO which led to a better lubricating performance with lower ice adhesion strength of the as-prepared samples.

Regarding the LPEG and PEG impregnated structures during the repeated tests, the ice adhesion strength of LPEG samples always increased to the values of their corresponding porous metallic structures, even on the POTS- and PW-coated samples. The reason is that the liquid phase of LPEG and higher solubility with water made it easier to deplete during the de-icing process as compared to the solid PEG. With the faster consumption of LPEG, the ice adhesion strength increased instantly with the receding of the unfrozen quasi-liquid layer and enhanced mechanical interlocking once the porous metallic surfaces were exposed to the water or ice. The situation of PEG-PIPMS was different as the solid nature led to a much slower consumption of PEG during the detachment of the ice block. Meanwhile, the solubility of PEG was less than that of LPEG, and the slower reduction of the over-covered PEG layer expected a sufficient amount of the quasi-liquid layer at the ice/structure interfaces that maintained the ice adhesion strength at a low level even after 50 cycles. Meanwhile, the PEG/POTS and PEG/PW demonstrated better water repellency than PEG/Cu. The ice adhesion strength of PEG/Cu increased to around 200 to 300 kPa after 20 icing/de-icing cycles, while the values of PEG/POTS increased to around 40 kPa at the 5th cycle, and increased to 50 to 60 kPa in the following repeated tests. The ice adhesion strength of PEG/PW increased slowly from around 20 kPa to less than 60 kPa even after the 50th test. The ice adhesion strength of the tested PEG-PIPMSs was only around 20% of their dry structures. Through the comparison with previous results of SLIPSs, the (ethylene glycol)-impregnated SLIPSs with porous Cu structure lost almost all the impregnated anti-freezing liquid and ice adhesion strength reached the value of porous Cu substrates [31]. However, in this study, the PEG/Cu had much better performance in both impregnation maintaining capacity and keeping ice adhesion low after 50 cycles. The ice adhesion strength increased to 232.1± 90.4 kPa, compared to the larger than 600 KPa of porous Cu. The mass loss rate of PEG/Cu was 72.7%, compared to nearly 100% consumption of ethylene glycol for SLIPSs with the liquid anti-freezing agent in our previous work [31]. The above comparison proved the advances of phase changeable PEG surfaces in improving long-term icephobicity and maintaining capacity of the impregnated PCMs.

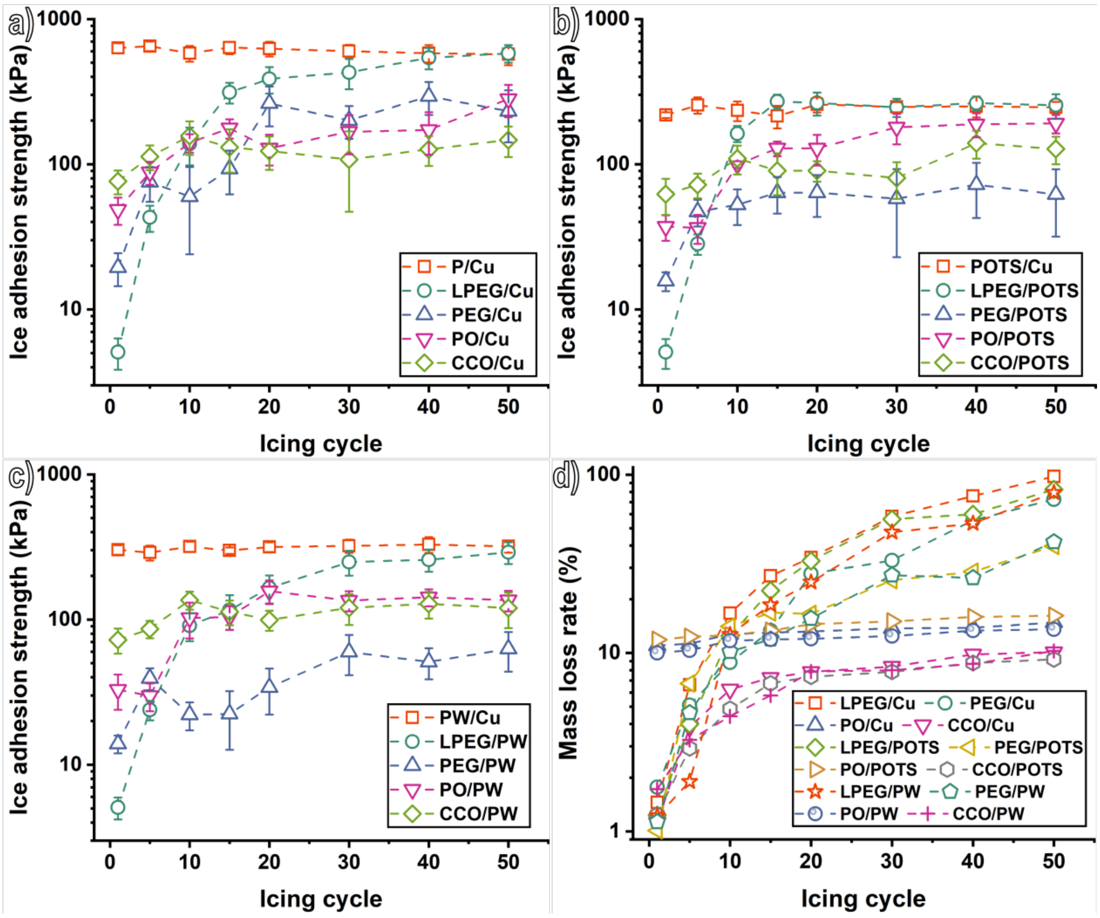

**Figure 4** Ice adhesion strengths in 50 icing/de-icing cycles on (a) Cu-based dry components and PIPMSs; (b) POTS-based dry components and PIPMSs; and (c) PW-based dry components and PIPMSs; (d) mass-loss rate of the PIPMSs in 50 cycles of ice adhesion strength test.

For the oil-PIPMSs, a similar trend between PO-PIPMSs and CCO-PIPMSs was observed, compared to that between LPEG-PIPMSs and PEG-PIPMSs. In the first several test cycles, the

PO-PIPMSs always had lower ice adhesion strength than the CCO-PIPMSs for all three porous structures. But the increase of ice adhesion of PO-PIPMSs was faster which led to higher values than CCO-PIPMSs after 10 to 15 icing/de-icing cycles until the end of the test. However, both of them still had lower ice adhesion strength (maintaining the icephobicity) than their corresponding porous metallic structures. Moreover, the POTS and PW layer led to the longer icephobicity, and the ice adhesion strength of PO/POTS, CCO/POTS, PO/PW, and CCO/PW were 190.9 ± 27.9 kPa, 127.2 ± 27.5 kPa, 135.9 ± 21.9 kPa, and 120.2 ± 32.3 kPa after 50 icing/de-icing tests (around 30% of the corresponding dry porous structures), respectively. These results demonstrate that the solid oil layer did have the lubricating capability to reduce ice adhesion. Meanwhile, due to the lower freezing point of CCO than PO, the PO was easier to be consumed during the ice detachment than CCO which led to a much slower depletion speed of CCO than that of PO. Also, this fact ensured that CCO-PIPMSs always had a lower ice adhesion than PO-PIPMSs in the latter half of the tests. Table 2 summarises the ice adhesion strength of PIPMSs in the repeated tests and the values from the references. On the one hand, the tested PIPMs had similar or even lower ice adhesion strength with much more icing/de-icing cycles than references [19, 21, 22, 30, 31, 33, 38, 44, 45]. For example, the ice adhesion strength of the as-prepared and tested PEG/POTS were 15.7±2.3 kPa and 61.9±30.2 kPa with 50 icing/de-icing cycles. The ice adhesion of PEG-impregnated porous polymers in reference increased from 40-90 kPa to 60-100 kPa after 7 icing/de-icing cycles [38]. On the other hand, the porous substrates from references were normally based on soft polymers or fragile materials which were not as robust as the porous metallic structures of PIPMSs [44, 45]. Moreover, part of the references did not evaluate the maintaining capacity of the impregnated materials during the icing/de-icing cycles. The detailed comparison of ice adhesion strength and other properties in this study and references was summarized in Table S3 in the supporting information.

Figure 4d summarises the consumption of the impregnated PCMs during the 50 times tests of ice adhesion strength. Although the mass loss rate of LPEG-PIPMSs and PEG/Cu still reached around or larger than 90%, the consumption of other PEG-PIPMSs and PO- or CCO-PIPMSs was reduced to around or less than 40%, 15%, and 9% respectively. The maintenance of the impregnated PCMs was enhanced more effectively as compared to the previous results [16, 31]. Even after 50 icing/de-icing cycles, the icephobic performance of most of the PEG-PIPMSs and all the oil-PIPMSs was demonstrated as the ice adhesion strengths stayed much lower than 100 kPa. More importantly, the values of ice adhesion strength and mass loss rate after 50 icing/de-icing cycles of PO/Cu, PO/POTS, and PO/PW were still similar (also for CCO/Cu, CCO/POTS, and CCO/PW), which showed different trend from our previous results for SLIPSs with liquid oil impregnation (P/Cu substrates had much higher ice adhesion and oil consumption than the samples with POTS/Cu and PW/Cu substrates) [31]. This fact confirmed that the solid lubricants (PO and CCO) enhanced the maintaining capacity of impregnated PCMs and extended the long-term icephobicity of PIPMSs effectively.

**Table 2** The comparison of repeated ice adhesion strength evaluation with reference data.

| Description of structures or coatings | Ice adhesion of as-prepared samples/kPa | Ice adhesion of tested samples/kPa |
|---|---|---|
| The present work (PEG/POTS) | 15.7±2.3 | 61.9±30.2<br>(50 cycles) |
| The present work (PEG/PW) | 13.9±1.9 | 62.8±19.1<br>(50 cycles) |
| The present work (PO/POTS) | 37.1±7.5 | 190.9±27.9<br>(50 cycles) |
| The present work (PO/PW) | 32.8±8.9 | 135.9±21.9<br>(50 cycles) |
| The present work (CCO/POTS) | 62.1±17.3 | 127.2±27.5<br>(50 cycles) |
| The present work (CCO/PW) | 72.5±14.3 | 120.2±32.8<br>(50 cycles) |
| Liquid-impregnated metallic structures [31] | 1-90 | 20-600 (50 cycles) |

| | | |
|---|---|---|
| Silicone oil impregnated in the electrochemical etched and functionalised porous surface of Mg alloy [44] | 45-68 | 58-140 (18 cycles) |
| Perfluoropolyether impregnated in the porous silicon wafer surfaces with superhydrophobic coatings [45] | 9-12 | 70-330 (20 cycles) |
| Silicone oil impregnated in the expanded network of cross-linked silicone resins [22] | 7-8 | 90-155 (13 cycles) |
| Perfluoropolyether-impregnated fluorinated polymer [19] | 3-7 | 20-40 (7 cycles) |
| Liquid paraffin-impregnated porous PDMS polymer coatings [21] | 20-60 | 40-70 (15 cycles) |
| Perfluoropolyether-impregnated $TiO_2$ nanotube arrays [30] | 36-80 | N/A |
| PEG-impregnated porous PDMS polymer coatings [38] | 40-90 | 60-100 (7 cycles) |
| PEG-impregnated porous PDMS polymer coatings [33] | 60-117 | 58-115 (3 cycles) |
| Silicone oil-impregnated porous PVDF polymer coating [46] | 19-32 | 20-58 (3 cycles) |

### 3.4 Durability investigation of PIPMSs

Figure 5 shows the surface morphology of the as-prepared and tested (after 50 times ice adhesion strength tests) PEG-PIPMSs, characterised by a 3D profilometer. It was clear that the as-prepared surface (Figure 5a) was quite smooth with full coverage of PCMs. The surface became much rougher due to the consumption of impregnated PCMs. However, the tested surface in Figure 5b is different from the porous metallic structures in Figure S4a of the supporting information, which indicates a good maintaining capacity of PEG in PEG-PIPMSs. This fact led to the existence of the unfrozen quasi-liquid layer on the surfaces even after 50 icing/de-icing cycles. Also, due to the solid state of CCO, the surface morphologies of the as-prepared and the tested CCO-PIPMSs are similar to those of PEG-PIPMSs in Figures 5a and 5b which remained the solid lubricating effect of the CCO-impregnated surfaces during the 50 icing/de-icing cycles.

The characterization was performed at room temperature which made LPEG and PO in the liquid phase. Due to the optical transparency of the thin-layer LPEG and PO, the changes in liquid surface morphology were not available and only the surface morphology of the porous metallic structures was presented. The surface morphology of LPEG- and PO-PIPMSs before and after the repeated icing/de-icing tests were summarised in Figure S4 of the supporting information.

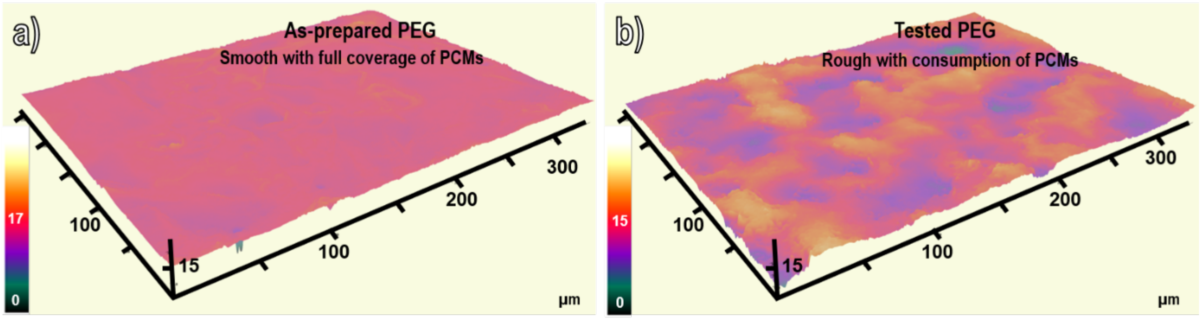

**Figure 5** Surface morphology of the PIPMSs (a) as-prepared PEG samples, and (b) tested PEG samples, characterised by a Zeta-20 optical profilometer.

Figure 6a summarises the icing time and icing phenomena of the as-prepared and tested PIPMSs. In general, three icing phenomena were observed in this study, which are the transparent icing process, supercooled icing process, and nonfrozen supercooled liquid phase. The transparent icing process referred to the phenomenon that icing happened once the droplet was added onto the surface and kept transparent. The supercooled icing process was the phenomenon in that no icing occurred at the beginning while the droplet was kept in the transparent liquid phase. At a certain point, the droplet changed from transparent to opaque suddenly, and then the icing started from the bottom and grew to the top until the end of the icing process. The third type, the supercooled liquid phase, did not contain any icing phenomenon during the 10-minute recording period, while the droplet was always kept in the transparent liquid phase. To show the above phenomena better, Video S1 to S3 are available in the supporting information.

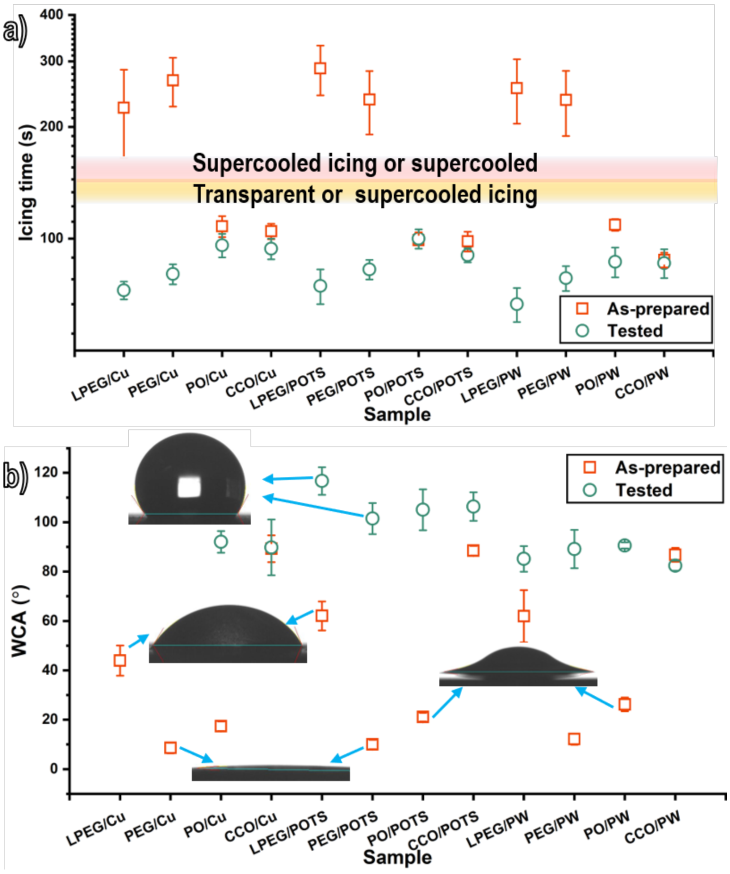

**Figure 6** (a) Icing time and icing phenomena of water droplet icing experiment and (b) WCA of different PIPMSs before and after the 50 times tests of ice adhesion strength.

For the as-prepared LPEG-PIPMSs and PEG-PIPMSs, due to the existence of a quasi-liquid layer, the icing time was increased to the range of 200 ~ 300s with the supercooled icing phenomena or always kept the supercooled liquid phase during the 10 minutes test. After the repeated ice adhesion tests, the surface droplet icing times decreased to the range from 66 s to 83 s with the transparent or occasional supercooled icing process because of the consumption of the impregnated PCMs and the receding of the quasi-liquid layer. Due to the better PCM maintaining capacity, the PEG-PIPMSs always had longer icing time than LPEG-PIPMSs for all porous structures. Regarding the PO-PIPMSs and CCO-PIPMSs, both of the as-prepared and tested samples mainly showed in the transparent icing process with the icing time in the range from the 80s to 110s. In comparison with the values from references, besides the marked extension of icing time, PIPMSs also had the potential to change the icing behaviours and prevent ice formation [26, 47]. Due to the smoother surfaces, some as-prepared samples had longer icing times than their tested samples, such as PO/Cu, CCO/Cu, CCO/POTS, and PO/PW. The above results also proved the importance and advances of the unfrozen quasi-liquid layer and solid lubricant surface.

Figure 6b shows the WCAs of the as-prepared and tested PIPMSs. The WCAs of the three dry porous structures can be found from our previous work, which was 128.5 ± 7.3° for POTS/Cu and 123.2 ± 6.2° for PW/Cu, but not measurable due to the hydrophilicity of P/Cu, respectively. For the as-prepared LPEG-PIPMSs, the WCAs fell in the range from 40° to 60° which was led by the hybrid effect of hydrophilic liquid LPEG, gravity, and the different hydrophobicity of the dry porous structures (as-prepared, POTS- and PW-treated structures). After repeated tests, due to the large consumption of LPEG, the WCAs became close to the values of their corresponding dry porous structures. Regarding the PEG-PIPMSs, due to the hydrophilicity and the full coverage of PEG, the WCAs were quite low at around or lower than 10°. After the test, the WCAs increased to 101.5 ± 6.3° (PEG/POTS) and 89.1 ± 7.8° (PEG/PW), similar to those of their dry porous structures, which was attributed to the direct contact between water and the porous Cu surface or the hydrophobic layers. For the PO-PIPMSs, the WCA distributed in the range from 18° to 22° at room temperature with a distorted droplet shape due to the difference in surface tension between water and liquid oil. Because of the consumption of the impregnated PO, water contacted the porous structures directly after the repeated icing/de-icing tests, and the values of WCA became similar to their dry structures after the test (92.1 ± 4.4° for PO/Cu, 105.0 ± 8.3° for PO/POTS, and 90.6 ± 1.2° for PO/PW). Regarding the CCO-PIPMSs, due to the full coverage of solid coconut oil before and after the test, there were no obvious changes in WCA as shown in Figure 6b (mainly from 80° to 90°), which accorded with the changing trend of ice adhesion for CCO-PIPMSs. The ice adhesion and oil consumption for all the CCO-PIPMSs always had similar values during the entire 50 icing/de-icing cycles.

The above results are in good agreement with the previous discussion about the variations in droplet icing time and icing phenomena.

### 3.5 Analysis of ice/PCM interfaces

Based on the above hypotheses and experimental verification, Figure 7 illustrates the phase changeable interfacial interactions between ice and PCMs, as well as the ice attachment and detachment behaviours. The theory of the quasi-liquid layer on the lubricating properties of ice suggests that a liquid-like layer exists on the ice surfaces [48-52]. The situations of LPEG- and PEG-PIPMSs in Figure 7a are quite similar to this theory. When the supercooled droplets or ice contact with the PIPMS surfaces, part of LPEG or PEG could be dissolved to form an unfrozen liquid layer at the interface (shown in Figure 7a). This interfacial interaction (unfrozen liquid layer) always offered good mobility and weak interaction. The quasi-liquid layer contributed to the low ice adhesion strength of the as-prepared LPE-PIPMSs (less than 5 kPa) and PEG-PIPMSs (less than 15 kPa). Meanwhile, compared to the low-viscosity anti-freezing agent in other SLIPSs [16, 31], the low solubility of LPEG and PEG in the water reduced the consumption of the impregnated materials at the interface. The high viscosity of LPEG and the solid phase of PEG also resulted in restrained depletion of PCMs when the ice was removed from the surface. Thus, PIPMSs still had low ice adhesion strength even after 50 icing/de-icing cycles, such as tested PEG/POTS with ice adhesion strength of 62.0 ± 30.2 kPa. Furthermore, compared to LPEG-PIPMSs, the PEG-PIPMSs achieved better PCM maintaining capacity and long-term icephobicity due to the solid phase of PEG and much lower water solubility (see Figure S1). More importantly, the POTS and PW treatment gave the porous structures effective water repellency, which further weakened the contact between PEG and ice/water. Even after 50 times tests, the PEG/POTS and PEG/PW still had low ice adhesion strength and good PEG storage, compared to PEG/Cu. The icing initiation position always started on the PEG surface with a quasi-liquid layer. Meanwhile, through comparison (in Section 3.3) between PEG/Cu and the results from our previous work, even without any surface functionalisation, the phase changeable PEG surface improved the long-term icephobicity and maintaining capacity of PEG effectively.

For the PO and CCO-PIPMSs, the contact between ice and PIPMSs occurred on the PCM surface. Although the PCMs (PO and CCO) stayed in the solid phase at subzero freezing environments, the surface still retained lubricating capability, which could be summarized as the solid lubricant effect. When the shear force was applied, a solid lubricant layer was presented at the ice/PIPMS interface (in Figure 7b). The ice adhesion strength was reduced also due to the solid lubricant effect. Besides keeping the ice adhesion at a low level during the cycle tests, the solid phase of lubricants dramatically improved the maintaining capacity of impregnated solid oils, compared to the liquid oil used in traditional SLIPSs. For example, less than 10% of CCO was consumed after 50 icing/de-icing tests of CCO/POTS. More importantly, there were no obvious differences in ice adhesion strength and PCMs (for PO and CCO) consumption among PO/Cu, PO/POTS, and PO/PW (or CCO/Cu, CCO/POTS, and CCO/PW) after 50 icing/de-icing cycles. This trend illustrated that the icing initiation position always started at the solid lubricant layer during the entire icing/de-icing tests, while the porous structure was covered by PO or CCO at subzero temperature. These facts proved that the impregnation of solid lubricant extended the icephobic durability effectively, compared to that of SLIPSs [22, 31].

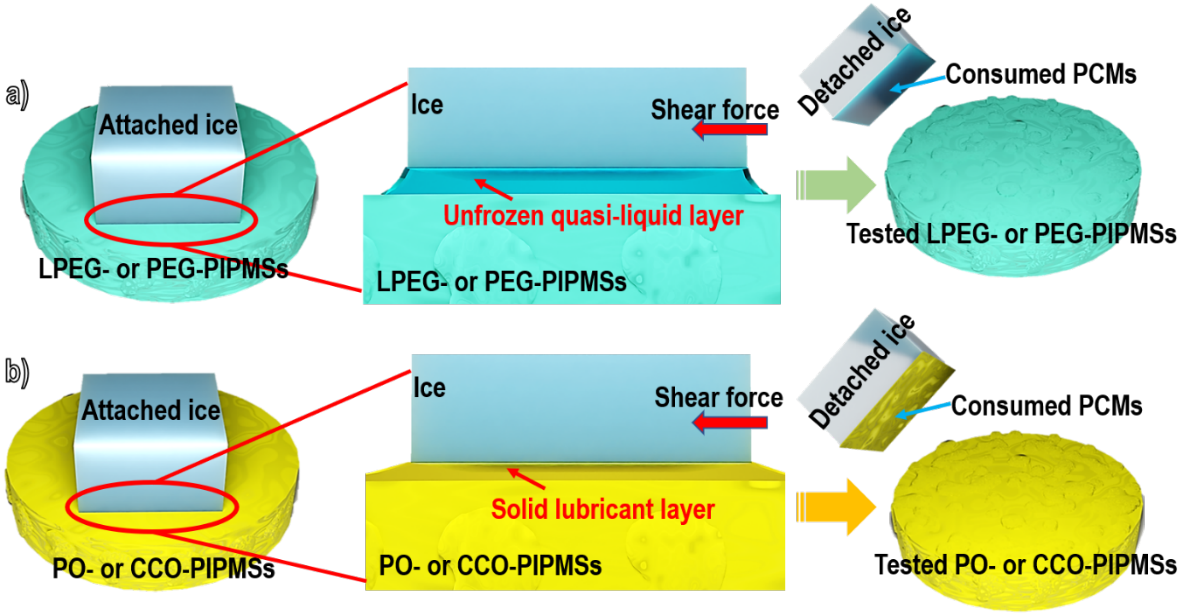

**Figure 7** Schematic illustration of ice attachment, ice/PIPMSs interfaces, and ice-detachment on PIPMSs for (a) LPEG- and PEG-PIPMSs, (b) PO- and CCO-PIPMSs.

Through the above experimental exploration and theoretical analysis, the existence of quasi-liquid layers and solid lubricant layers on PIPIMSs transferred the ice initiation and attaching position from the dry porous surfaces to the smooth phase change surfaces, delaying the ice nucleation and weakening the ice adhesion. The consumption of PCMs during the repeated icing/de-icing cycles was markedly restrained which improved the long-term icephobic performance. The broken and receding of the phase change surfaces caused the slight loss of icephobicity. Thus, further efforts need to be paid to the optimisation of the porous structural design, synergetic development of phase changeable icephobic surfaces with thermal systems, functionalising PCMs, modifying the molecular chain of the elastic polymers by PCMs, etc.

## 4. Conclusions

To address the rapid liquid depletion of icephobic SLIPSs [19-22], durable phase changeable icephobic surfaces were developed based on the PCM-impregnated porous metallic structures (PIPMSs) in this study, and the interfacial interaction at the ice/solid interface was tailored. Phase change models of unfrozen quasi-liquid layer (LPEG-/PEG-PIPMSs) and solid lubricant layer (PO-/CCO-PIPMSs) were proposed and revealed the interfacial anti/de-icing mechanisms. The unfrozen liquid layer of the quasi-liquid route would prevent ice formation even after 20 times icing cycles in an extremely humid environment (good humid tolerance), and delay icing time to around 300 seconds with the changes in icing phenomena from fast transparent icing to slower supercooled icing, further to the unfrozen supercooled liquid process. Besides obtaining ultra-low ice adhesion strength of as-prepared PIPMSs (less than 5 kPa), the tested PIPMSs achieved excellent maintaining capacity of the impregnated PCMs (consumption less than 10% for solid lubricating PIPMSs) after 50 icing/de-icing cycles, while the ice adhesion strength was kept at a low level (less than 60 kPa). With the analysis of surface wettability and droplet icing, phase change models of the unfrozen quasi-liquid layer and solid lubricant layer at the ice/PIPMSs interfaces were established.

In comparison with the references (Table 2 in the manuscript and Table S3 in supporting information), the proposed PIPMSs in this study demonstrated lower ice adhesion strengths with robust porous metallic structures (mainly soft polymer in references) [19, 21, 22, 30, 31, 33, 38, 46, 53, 54]. The evaluation of PCM consumption, much longer icing/de-icing cycles, and robust porous metallic structures offered strong evidence of the advances of PIPMSs. More importantly, through the comparison with the previously reported work, the phase changeable icephobic surfaces demonstrated significantly enhanced long-term icephobicity. The phase changeable icephobic surfaces from the new strategy of PIPMS will inspire research about the interfacial study of ice/structure, slippery icephobic surfaces, and phase change materials. Future work about the innovation of porous metallic structures and the development of composite/functionalised PCMs have good potential to develop applicable slippery icephobic surfaces.

## Acknowledgements

The authors acknowledge the use of facilities at the Nanoscale and Microscale Research Centre of the University of Nottingham, this research was supported in part by the Engineering and Physical Sciences Research Council [grant number EP/L022494/1], as well as the National Natural Science Foundation of China [grant number 52174345 and 52064032].

## CRediT authorship contribution statement

**D. Yang**: Conceptualization; Data curation; Investigation; Methodology; Writing – original draft. **R. Bao**: Methodology; Writing – review & editing. **A.T. Clare**: Supervision; Writing – review & editing. **K. Choi**: Supervision; Writing – review & editing. **X. Hou**: Conceptualization; Funding acquisition; Supervision; Writing – review & editing.

## Declaration of Competing Interest

The authors declare that they have no known competing financial interests or personal relationships that could have appeared to influence the work reported in this paper.

## References

[1] Newton, D. W., An integrated approach to the problem of aircraft icing. *J Aircr.* **1978,** *15* (6), 374-380.

[2] Gent, R. W.; Dart, N. P.; Cansdale, J. T., Aircraft icing. *Philosophical Transactions of the Royal Society of London. Series A: Mathematical, Physical and Engineering Sciences.* **2000,** *358* (1776), 2873-2911.

[3] Pohlman, J. C.; Landers, P. J. I. T. o. P. A., Present state-of-the-art of transmission line icing. *IEEE Trans. Power Appar. Syst.* **1982,** (8), 2443-2450.

[4] Parent, O.; Ilinca, A., Anti-icing and de-icing techniques for wind turbines: Critical review. *Cold Reg Sci Technol.* **2011,** *65* (1), 88-96.

[5] Heyun, L.; Xiaosong, G.; Wenbin, T., Icing and anti-icing of railway contact wires. *Reliab. Eng. Syst. Saf.* **2012**, 295-314.

[6] Li, T.; Li, J. In *Analysis of icing accident in South China power grids in 2008 and it's countermeasures*, CIRED 2009-20th International Conference and Exhibition on Electricity Distribution-Part 1, IET: 2009; pp 1-4.

[7] Cao, Y.; Tan, W.; Wu, Z., Aircraft icing: An ongoing threat to aviation safety. *Aerosp Sci Technol.* **2018,** *75*, 353-385.

[8] Green, S. In *A study of US inflight icing accidents and incidents, 1978 to 2002*, 44th AIAA Aerospace Sciences Meeting and Exhibit, 2006; p 82.

[9] Ryerson, C. C., Ice protection of offshore platforms. *Cold Reg Sci Technol.* **2011,** *65* (1), 97-110.

[10] Huang, X.; Tepylo, N.; Pommier-Budinger, V.; Budinger, M.; Bonaccurso, E.; Villedieu, P.; Bennani, L., A survey of icephobic coatings and their potential use in a hybrid coating/active ice protection system for aerospace applications. *Prog. Aerosp. Sci.* **2019,** *105*, 74-97.

[11] Irajizad, P.; Nazifi, S.; Ghasemi, H., Icephobic surfaces: Definition and figures of merit. *Adv. Colloid Interface Sci.* **2019,** *269*, 203-218.

[12] Yang, D.; Haworth, L.; Agrawal, P.; Tao, R.; McHale, G.; Torun, H.; Martin,

J.; Luo, J.; Hou, X.; Fu, Y., Dynamic mitigation mechanisms of rime icing with propagating surface acoustic waves. *Langmuir.* **2022,** *38* (37), 11314-11323.

[13] Yang, D.; Tao, R.; Hou, X.; Torun, H.; McHale, G.; Martin, J.; Fu, Y., Nanoscale “Earthquake” Effect Induced by Thin Film Surface Acoustic Waves as a New Strategy for Ice Protection. *Adv. Mater. Interfaces.* **2021,** *8* (2), 2001776.

[14] Kim, P.; Wong, T.-S.; Alvarenga, J.; Kreder, M. J.; Adorno-Martinez, W. E.; Aizenberg, J., Liquid-infused nanostructured surfaces with extreme anti-ice and anti-frost performance. *ACS nano.* **2012,** *6* (8), 6569-6577.

[15] Ozbay, S.; Yuceel, C.; Erbil, H. Y., Improved icephobic properties on surfaces with a hydrophilic lubricating liquid. *ACS Appl. Mater. Interfaces.* **2015,** *7* (39), 22067-22077.

[16] Kreder, M. J.; Alvarenga, J.; Kim, P.; Aizenberg, J., Design of anti-icing surfaces: smooth, textured or slippery? *Nat. Rev. Mater.* **2016,** *1* (1), 1-15.

[17] Jamil, M. I.; Ali, A.; Haq, F.; Zhang, Q.; Zhan, X.; Chen, F., Icephobic strategies and materials with superwettability: design principles and mechanism. *Langmuir.* **2018,** *34* (50), 15425-15444.

[18] He, Z.; Zhuo, Y.; Zhang, Z.; He, J., Design of icephobic surfaces by lowering ice adhesion strength: A mini review. *Coatings.* **2021,** *11* (11), 1343.

[19] Wei, C.; Jin, B.; Zhang, Q.; Zhan, X.; Chen, F., Anti-icing performance of super-wetting surfaces from icing-resistance to ice-phobic aspects: Robust hydrophobic or slippery surfaces. *J. Alloys Compd.* **2018,** *765*, 721-730.

[20] Latthe, S. S.; Sutar, R. S.; Bhosale, A. K.; Nagappan, S.; Ha, C.-S.; Sadasivuni, K. K.; Liu, S.; Xing, R., Recent developments in air-trapped superhydrophobic and liquid-infused slippery surfaces for anti-icing application. *Prog. Org. Coat.* **2019,** *137*, 105373.

[21] Zhuo, Y.; Wang, F.; Xiao, S.; He, J.; Zhang, Z., One-step fabrication of bioinspired lubricant-regenerable icephobic slippery liquid-infused porous surfaces. *ACS omega.* **2018,** *3* (8), 10139-10144.

[22] Coady, M. J.; Wood, M.; Wallace, G. Q.; Nielsen, K. E.; Kietzig, A.-M.; Lagugné-Labarthet, F. o.; Ragogna, P. J., Icephobic behavior of UV-cured polymer networks incorporated into slippery lubricant-infused porous surfaces: Improving SLIPS durability. *ACS*

*Appl. Mater. Interfaces.* **2018,** *10* (3), 2890-2896.

[23] Zhang, S.; Huang, J.; Cheng, Y.; Yang, H.; Chen, Z.; Lai, Y., Bioinspired surfaces with superwettability for anti-icing and ice-phobic application: concept, mechanism, and design. *Small.* **2017,** *13* (48), 1701867.

[24] Heydarian, S.; Jafari, R.; Momen, G., Recent progress in the anti-icing performance of slippery liquid-infused surfaces. *Prog. Org. Coat.* **2021,** *151*, 106096.

[25] Khammas, R.; Koivuluoto, H., Durable Icephobic Slippery Liquid-Infused Porous Surfaces (SLIPS) Using Flame-and Cold-Spraying. *Sustainability.* **2022,** *14* (14), 8422.

[26] Mahmut, T.; Memon, H.; Xu, F.; Ahmed, I.; Hou, X., Electrospun nanofibre membrane based transparent slippery liquid-infused porous surfaces with icephobic properties. *Colloids Surf. A Physicochem. Eng. Asp.* **2020,** *585*, 124177.

[27] S. Aghdam, A.; Cebeci, F. C., Tailoring the icephobic performance of slippery liquid-infused porous surfaces through the LbL method. *Langmuir.* **2020,** *36* (46), 14145-14154.

[28] Irajizad, P.; Hasnain, M.; Farokhnia, N.; Sajadi, S. M.; Ghasemi, H., Magnetic slippery extreme icephobic surfaces. *Nat. Commun.* **2016,** *7* (1), 1-7.

[29] Haikun, Z.; Shinan, C.; Yuanyuan, Z., Anti-icing & icephobic mechanism and applications of superhydrophobic/ultra slippery surface. *Prog. Chem.* **2017,** *29* (1), 102.

[30] Yan, Y.; Wang, J.; Gao, J.; Ma, Y., TiO2-based slippery liquid-infused porous surfaces with excellent ice-phobic performance. *Colloids Surf. A Physicochem. Eng. Asp.* **2022,** *654*, 129994.

[31] Yang, D.; Bao, R.; Clare, A. T.; Choi, K.-S.; Hou, X., Hydrophobically/oleophilically guarded powder metallurgical structures and liquid impregnation for ice mitigation. *Chem. Eng. J.* **2022,** *446*, 137115.

[32] Raoux, S., Phase change materials. *Annu. Rev. Mater.* **2009,** *39*, 25-48.

[33] Chen, D.; Gelenter, M. D.; Hong, M.; Cohen, R. E.; McKinley, G. H., Icephobic surfaces induced by interfacial nonfrozen water. *ACS Appl. Mater. Interfaces.* **2017,** *9* (4), 4202-4214.

[34] Wang, X.; Huang, J.; Guo, Z., Overview of the development of slippery surfaces: Lubricants from presence to absence. *Adv. Colloid Interface Sci.* **2022**, 102602.

[35] Zhu, K.; Li, X.; Su, J.; Li, H.; Zhao, Y.; Yuan, X., Improvement of anti-icing properties of low surface energy coatings by introducing phase-change microcapsules. *Polym.Eng. Sci.* **2018,** *58* (6), 973-979.

[36] Yuan, Y.; Xiang, H.; Liu, G.; Liao, R., Fabrication of phase change microcapsules and their applications to anti-icing coating. *Surf. Interfaces.* **2021,** *27*, 101516.

[37] Yancheshme, A. A.; Allahdini, A.; Maghsoudi, K.; Jafari, R.; Momen, G., Potential anti-icing applications of encapsulated phase change material–embedded coatings; a review. *J Energy Storage.* **2020,** *31*, 101638.

[38] Shamshiri, M.; Jafari, R.; Momen, G., Icephobic properties of aqueous self-lubricating coatings containing PEG-PDMS copolymers. *Prog. Org. Coat.* **2021,** *161*, 106466.

[39] Shamshiri, M.; Jafari, R.; Momen, G., An intelligent icephobic coating based on encapsulated phase change materials (PCM). *Colloids Surf. A Physicochem. Eng. Asp.* **2022,** *655*, 130157.

[40] Wang, J.; Wu, M.; Liu, J.; Xu, F.; Hussain, T.; Scotchford, C.; Hou, X., Metallic skeleton promoted two-phase durable icephobic layers. *J. Colloid Interface Sci.* **2021,** *587*, 47-55.

[41] Zehui, Z.; Zelinlan, W.; Guang, L.; Dengke, C.; Kaiteng, Z.; Yantong, Z.; Jichen, C.; Shize, S.; Xiaolin, L.; Huawei, C., Liquid-like slippery surface with passive-multi active strategy integration for anti-icing/de-icing. *Chem. Eng. J.* **2023,** *474*, 145541.

[42] Wu, D.; Ma, L.; Zhang, F.; Qian, H.; Minhas, B.; Yang, Y.; Han, X.; Zhang, D., Durable deicing lubricant-infused surface with photothermally switchable hydrophobic/slippery property. *Materials & Design* **2020,** *185*, 108236.

[43] Fletcher, N. H., Size effect in heterogeneous nucleation. *Chem. Phys.* **1958,** *29* (3), 572-576.

[44] Liu, C.; Li, Y.; Lu, C.; Liu, Y.; Feng, S.; Liu, Y., Robust slippery liquid-infused porous network surfaces for enhanced anti-icing/deicing performance. *ACS Appl. Mater. Interfaces.* **2020,** *12* (22), 25471-25477.

[45] Tan, X.; Zhang, Y.; Liu, X.; Xi, S.; Yan, Z.; Liu, Z.; Shi, T.; Liao, G., Employing micro pyramidal holes and porous nanostructures for enhancing the durability of

lubricant-infused surfaces in anti-icing. *Surface and Coatings Technology* **2021,** *405*, 126568.

[46] Cui, W.; Pakkanen, T. A., Icephobic performance of one-step silicone-oil-infused slippery coatings: Effects of surface energy, oil and nanoparticle contents. *J. Colloid Interface Sci.* **2020,** *558*, 251-258.

[47] Wu, M.; Wang, J.; Ling, S.; Wheatley, R.; Hou, X., Microporous metallic scaffolds supported liquid infused icephobic construction. *J. Colloid Interface Sci.* **2023,** *634*, 369-378.

[48] Jellinek, H., Liquidlike layers on ice. *J. Appl. Phys.* **1961,** *32* (9), 1793-1793.

[49] Jellinek, H. H. G., Liquid-like (transition) layer on ice. *J. Colloid Interface Sci.* **1967,** *25* (2), 192-205.

[50] Gilpin, R., A model of the "liquid-like" layer between ice and a substrate with applications to wire regelation and particle migration. *J. Colloid Interface Sci.* **1979,** *68* (2), 235-251.

[51] Döppenschmidt, A.; Butt, H.-J., Measuring the thickness of the liquid-like layer on ice surfaces with atomic force microscopy. *Langmuir.* **2000,** *16* (16), 6709-6714.

[52] Goertz, M.; Zhu, X.-Y.; Houston, J., Exploring the liquid-like layer on the ice surface. *Langmuir.* **2009,** *25* (12), 6905-6908.

[53] Rao, Q.; Zhang, J.; Zhan, X.; Chen, F.; Zhang, Q., UV-driven self-replenishing slippery surfaces with programmable droplet-guiding pathways. *Journal of Materials Chemistry A* **2020,** *8* (5), 2481-2489.

[54] Gao, S.; Liu, B.; Peng, J.; Zhu, K.; Zhao, Y.; Li, X.; Yuan, X., Icephobic durability of branched PDMS slippage coatings co-cross-linked by functionalized POSS. *ACS Appl. Mater. Interfaces.* **2019,** *11* (4), 4654-4666.

## Figure captions:

**Figure 1** Schematic illustration of the preparation of PIPMSs.

**Figure 2** ESEM characterisation of the process for (a) water condensation and (b) ice nucleation and growth on dry porous Cu structures.

**Figure 3** Accretion of rime ice on various PIPMSs in 20 cycles of aerosol icing experiment.

**Figure 4** Ice adhesion strengths in 50 icing/de-icing cycles on (a) Cu-based dry components and PIPMSs; (b) POTS-based dry components and PIPMSs; and (c) PW-based dry components and PIPMSs; (d) mass-loss rate of the PIPMSs in 50 cycles of ice adhesion strength test.

**Figure 5** Surface morphology of the PIPMSs (a) as-prepared PEG samples, and (b) tested PEG samples, characterised by a Zeta-20 optical profilometer.

**Figure 6** (a) Icing time and icing phenomena of water droplet icing experiment and (b) WCA of different PIPMSs before and after the 50 times tests of ice adhesion strength.

**Figure 7** Schematic illustration of ice attachment, ice/PIPMSs interfaces, and ice-detachment on PIPMSs for (a) LPEG- and PEG-PIPMSs, (b) PO- and CCO-PIPMSs.

# Table captions:

**Table 1** Description and abbreviation of porous metallic structures and PIPMSs.

**Table 2** Physical properties of polyethylene glycol-200, polyethylene glycol-2000, peanut oil, and coconut oil (obtained in the specification from the supplier or references).